NACA

RESEARCH MEMORANDUM

for the

U. S. Air Force

LATERAL-STABILITY FLIGHT TEST OF A 0.125-SCALE ROCKET-PROPELLED MODEL OF THE McDONNELL F-101A AIRPLANE AT MACH NUMBERS FROM 1.0 TO 1.9

By James A. Hollinger and Lucille C. Coltrane

Langley Aeronautical Laboratory
Langley Field, Va.

NATIONAL ADVISORY COMMITTEE
FOR AERONAUTICS

WASHINGTON

NACA RM SL56D20

NATIONAL ADVISORY COMMITTEE FOR AERONAUTICS

RESEARCH MEMORANDUM

for the

U. S. Air Force

LATERAL-STABILITY FLIGHT TEST OF A 0.125-SCALE ROCKET-PROPELLED MODEL OF THE McDONNELL F-101A AIRPLANE AT MACH NUMBERS FROM 1.0 TO 1.9

By James A. Hollinger and Lucille C. Coltrane

SUMMARY

A rocket-propelled model of the McDonnell F-101A airplane was tested in free flight for its lateral stability characteristics. The 0.125-scale model was equipped with six pulse rockets to produce the lateral disturbances. The center of gravity was located at 17.3 percent of the mean aerodynamic chord.

The method of analysis was based on lateral-force and moment vector diagrams which were trigonometrically solved for the resultants.

The slope of the side-force curve C_{Y_β} varied little with speed, but remained at a value of about -1.0. The dihedral effect was adequate.

The model was statically stable but dynamically neutral. The roll damping was nearly constant through the speed range and agreed with some theoretical values.

INTRODUCTION

Rocket-model tests of the McDonnell F-101A airplane have been conducted by the Langley Pilotless Aircraft Research Division at the request of the U. S. Air Force. The purpose of the present test was to determine the lateral stability characteristics of the airplane at transonic and supersonic speeds. Lateral disturbances were produced by pulse rockets.

A previous test in the series presented longitudinal stability characteristics and drag data. (See ref. 1.) The present paper contains supersonic lateral-stability information of the F-101A. The test was made

without power but the drag of the engine and ducting system was simulated. A measurement of the mass-flow ratio was made.

SYMBOLS

a	total damping factor
Alt.	altitude, ft
b	wing span, ft
$\bar{c}$	mean aerodynamic chord, ft
$c_{1/2}$	cycles to damp to one-half amplitude
I_x	moment of inertia about body roll axis, slug-ft^2
I_z	moment of inertia about body yaw axis, slug-ft^2
I_{xz}	product of inertia, slug-ft^2
k_x	radius of gyration in YZ-plane, ft
k_y	radius of gyration in XZ-plane, ft
k_z	radius of gyration in XY-plane, ft
m	mass of model, slugs
M	test Mach number
p	rolling angular velocity, radians/sec
q	dynamic pressure, lb/sq ft
r	yawing angular velocity, radians/sec
R	Reynolds number
S	theoretical wing area, sq ft
V	velocity, ft/sec
v_e	equivalent lateral velocity, ft/sec

[redacted]

w/w_o	duct mass-flow ratio
α	angle of attack at model center of gravity, deg
β	angle of sideslip, deg
ϵ	inclination of principal axis, deg
μ_b	mass density parameter, $m/\rho Sb$
ρ	air density, slugs/cu ft
φ	roll angle, radians
ψ	angle of yaw, radians
ω	frequency of the Dutch roll oscillation, radians/sec
Ω_{C_Y}	phase angle of side-force coefficient to angle of sideslip, radians unless otherwise noted
Ω_p	phase angle of roll rate to angle of sideslip, radians unless otherwise noted
C_L	lift coefficient
C_Y	side-force coefficient
C_{L_α}	lift-curve slope
C_{l_p}	coefficient of rolling moment due to rolling velocity, $\frac{\partial C_l}{\partial\left(\frac{pb}{2V}\right)}$
C_{l_r}	coefficient of rolling moment due to yawing velocity, $\frac{\partial C_l}{\partial\left(\frac{rb}{2V}\right)}$
C_{l_β}	coefficient of rolling moment due to sideslip, $\frac{\partial C_l}{\partial \beta}$, per radian
C_{n_p}	coefficient of yawing moment due to rolling velocity, $\frac{\partial C_n}{\partial\left(\frac{pb}{2V}\right)}$
C_{n_r}	coefficient of yawing moment due to yawing velocity, $\frac{\partial C_n}{\partial\left(\frac{rb}{2V}\right)}$

[redacted]

C_{n_β} coefficient of yawing moment due to sideslip, $\frac{\partial C_n}{\partial \beta}$, per radian

$C_{n_{\dot{\beta}}}$ coefficient of yawing moment due to sideslipping velocity $\frac{\partial C_n}{\partial\left(\frac{\dot{\beta} b}{2V}\right)}$, per radian

C_{Y_β} coefficient of side force due to sideslip, $\frac{\partial C_Y}{\partial \beta}$

The symbol $|\ |$ represents the absolute magnitude of the quantity and is always taken to be positive.

A dot over a symbol indicates that the quantity has been differentiated with respect to time.

MODEL AND TESTS

A three-view drawing of the model is shown in figure 1 and physical characteristics of the model are given in table I. The center of gravity was located at 17.3 percent of the mean aerodynamic chord. The basic structure of the model consisted of longitudinal aluminum and steel bulkheads. Wooden fairings and plastic hatches formed the body contour.

The swept wing was constructed of aluminum-alloy plates and mahogany fillers. The wing thickness varied from 6.67 percent of the chord at the root to 5.71 percent at the tip. The sections were NACA airfoils modified by extending the chord 5 percent forward of the 16.04-percent chord line and adding 1.67-percent positive camber. There were stall plates (fences) located at about 70 percent of each semispan, and the wing had 1° positive incidence. An inboard trailing-edge extension of about 66 percent of the center-line chord tapered to zero percent chord near the center of each semispan.

The vertical-tail surface was constructed similarly to the wing and there was no rudder deflection. The swept horizontal tail, constructed of solid aluminum alloy, was fixed at a deflection of -0.4° to trim the model at a low positive lift coefficient.

An unswept inlet incorporating a boundary-layer bleed was located on the wing root. Internal ducting consisted of two separate ducts. An inner body in each duct duplicated the cross-sectional area of the engines and accessory housings at the proper location. The internal ducting did not duplicate that of the full-scale airplane behind the inner body, but the exit-to-entrance area ratio was designed to regulate

[redacted]

the mass flow to approximate the engine requirements at supersonic speeds. A minimum cross section was installed near each duct exit and three total-pressure tubes were mounted in one duct slightly forward of this minimum section to permit the calculation of internal drag at choked conditions. Since the base area of the afterburner did not duplicate that of the full-scale airplane, the base drag of the model was calculated from the static pressure on the base area. The average static-pressure variation over the flat base of one of the afterburners was measured by six manifolded static-pressure tubes.

The lateral disturbances were produced by six small rockets whose thrust produced a short lateral acceleration. The timing of these pulses placed two of them in the supersonic speed range and the remainder in the transonic and high subsonic speed ranges.

The model was flown at the Langley Pilotless Aircraft Research Station at Wallops Island, Va. It was boosted from a zero-length launcher with a 2.5-DS-59000 booster rocket. The booster burned out at a Mach number of about 2 and separated from the model, which was allowed to coast freely. The data obtained during the coasting phase are presented in this report. The booster adapter and drag flap were similar to those used on the model of reference 1. Figure 2(a) is a photograph of the model and figure 2(b) is a photograph of the model-booster combination prior to launching.

INSTRUMENTATION

A telemeter system recorded simultaneously and continuously the lateral-stability data and other information found for this test. The recorded channels containing the motional information were: accelerations in the transverse, normal, and longitudinal directions at the center of gravity; accelerations in the transverse and normal directions in the nose; rate of roll; angle of sideslip; and angle of attack. Also recorded were free-stream total pressure, duct total pressure, afterburner base pressure, wind-direction-vane base pressure, and a differential pressure taken in the duct to detect flow separation.

A rawinsonde released at the time of firing recorded the free-stream temperature and static pressure over the altitude range covered by the test. The velocity and position in space of the model were determined by a CW Doppler radar set and a radar tracking unit. The foregoing information is combined in figure 3 and is presented as dynamic pressure and Reynolds number plotted against test Mach number. In figure 4(a) the model mass density factor μ_b is shown, and in figure 4(b) the altitude is shown at which the full-scale airplane would have to fly to have the same mass parameter.

ANALYSIS

Throughout the test the model executed a continuous lateral motion which showed little damping; thus the time to damp to one-half amplitude was considered infinite. Two time histories of the motion are shown in figure 5. The model executed a motion appearing to have five degrees of freedom but computations based on three degrees of freedom gave an adequate analysis of the motion. The equations of motion use the body axis system of coordinates.

The frequency of the Dutch roll motion is shown in figure 6. The frequency was used to compute the lateral-static-stability parameter by the following equation which was written for one degree of freedom and which assumed that the center of gravity moved in a straight line:

$$C_{n_\beta} = \frac{I_Z}{qSb} \omega^2$$

The derivative C_{n_β} was also found by a three-degree-of-freedom analysis, and the difference in C_{n_β} shown by the two methods is a measure of the effect of neglecting the product of inertia terms, as shown in figure 7. The inclination of the principal axis, measured to be 4.2°, was used to compute the product of inertia.

The vector method of references 2 and 3 was used to compute C_{n_β} and the other lateral-stability derivatives with use of the equations shown in figure 7. The time vectors, such as the example given in figure 7 for one solution, constitute a three-degree-of-freedom analysis by using basic motional information such as the representative curves of the variation of side-force coefficient with angle of sideslip given in figure 8, and the slopes of these curves are given in (fig. 9). The primary vectorial data are presented in the following figures: C_{Y_β} (fig. 9), the Dutch roll frequency (fig. 6), the phase difference between the roll rate and the angle-of-sideslip oscillations and between the side-force coefficient and the angle-of-sideslip oscillations (fig. 10), and the amplitude ratio of the rate of roll to angle of sideslip (fig. 11). The phase angles in figure 10 include corrections required by the frequency response characteristics of the roll rate gyro. The individual points of the primary data plots were used in the vector analysis in order to show the full effect of their scatter on the derivatives computed.

The method allows the determination of two derivatives in each degree of freedom, whereas the third must be otherwise determined. The cross

derivatives, C_{l_r} and C_{n_p}, were assigned two values to show the effect of selecting them as the derivatives not found in the analysis.

The duct mass-flow ratio was measured by using the indication of three manifolded total-pressure tubes installed just ahead of a choking section at the exit of the duct.

RESULTS

The lateral derivatives are all presented as groups of data points. The results give a visual estimation of the accuracy of determining each derivative. Also shown are the effects of neglecting the cross derivatives or the product of inertia terms, as explained in the "Analysis" section. Generally, the change in the cross derivatives appears to produce a change in the results much smaller than the range of values covered because of the accuracy of the method.

The roll-damping derivative C_{l_p} is presented in figure 12, where the apparent scatter is mainly a result of the variation of Ω_p in figure 10. Theoretical values are shown as computed from references 4 and 5. The roll damping remained near the same level throughout the speed range and agreed with the theoretical values.

The dihedral-effect derivative, C_{l_β}, (fig. 13) shows little change in value with change of C_{l_r}.

The static lateral stability, figure 14, is shown for the two methods of computation and for the change in C_{n_p}. The values of C_{n_β} based on a one-degree-of-freedom analysis of the periods are slightly different from those found by the vector computations. The difference is a measure of the effect of neglecting the product-of-inertia terms. The change in C_{n_p} has a negligible effect on C_{n_β}.

Presented in figure 15 is the dynamic-lateral-stability derivative $C_{n_r} - C_{n_{\dot{\beta}}}$ which shows a greater effect of the change in C_{n_p}. The derivative $C_{n_r} - C_{n_{\dot{\beta}}}$ remains negative throughout the speed range, but the model motion showed little damping. The reason for little or no damping observed in the model motion was believed to be the large roll coupling due to the relatively large product of inertia. For the angle of attack of this test the out-of-phase yawing moment contributed by the product-of-inertia term

[redacted]

is of opposite sign and larger magnitude than that contributed by $C_{n_r} - C_{n_{\dot{\beta}}}$. (See fig. 7.)

The difference in the inertia characteristics of the model and airplane is shown in the following table:

	Rocket model	F-101A airplane
k_x/b	0.111	0.102
$k_y/\bar{c}$	1.548	1.092
k_z/b	0.405	0.290
ϵ, deg	4.2	3.0

The damping was computed for the model by substituting into the equations of motion both values given above for the inertia factors k_x/b, k_z/b, and ϵ. Values of damping and roll amplitude were found and are shown in figure 16 in the form used in reference 6 to specify military requirements. Giving the model the same inertia characteristics as the full-scale airplane made the damping approximately the same as that computed for the F-101A at the same Mach number. The calculation of the airplane damping placed the airplane at 47,000 feet in order to duplicate the mass-density ratio at which the model was flown. Also shown in figure 16 are results of calculations carried out at an arbitrary lower altitude picked to make the angles of attack nearer those of the model. Other results are shown at the same altitude for three lesser Mach numbers. The increase in damping parameter at the slower speeds is a result, not of a shorter time to damp, but of longer periods at these speeds.

In figure 17 there are presented some curves of the variation of lift coefficient with angle of attack, and the slope of the lift curve is presented in figure 18 where the lift-curve slope of the longitudinal control model (ref. 1) is compared with that of the present test. Figure 19 shows the variation of trim lift coefficient with Mach number.

The duct mass-flow ratio is presented in figure 20.

SUMMARY OF RESULTS

A flight test of a 0.125-scale model of the McDonnell F-101A airplane in the Mach number range from 1.0 to 1.9 gave the following results:

1. The model was statically stable and dynamically neutral although the dynamic stability derivative was negative.

[redacted]

2. The roll damping remained near the same level through the speed range tested and agreed well with some theoretical values.

3. There was an adequate dihedral effect.

4. The cross derivatives C_{n_p} and C_{l_r} were not determined, but their effects on the other derivatives were shown to be small.

5. The slope of the lateral-force curve C_{Y_β} varied slightly with speed; that is, C_{Y_β} dropped from -1.1 at a Mach number of 1.1 to a value of -0.9 at a Mach number of 1.9.

Langley Aeronautical Laboratory,
National Advisory Committee for Aeronautics,
Langley Field, Va., April 4, 1956.

James A. Hollinger

James A. Hollinger
Aeronautical Research Scientist

Lucille C. Coltrane

Lucille C. Coltrane
Mathematician

Approved:

Joseph A. Shortal

Joseph A. Shortal
Chief of Pilotless Aircraft Research Division

sam

[redacted]

REFERENCES

1. Hastings, Earl C., Jr., and Mitcham, Grady L.: Flight Determination of the Longitudinal Stability and Control Characteristics of a 0.125-Scale Rocket-Boosted Model of the McDonnell F-101A Airplane at Mach Numbers From 0.82 to 1.84. NACA RM SL55F24, U. S. Air Force, 1955.

2. Mitchell, Jesse L., and Peck, Robert F.: Investigation of the Lateral Stability Characteristics of the Douglas X-3 Configuration at Mach Numbers From 0.6 to 1.1 by Means of a Rocket-Propelled Model. NACA RM L54L20, 1955.

3. D'Aiutolo, Charles T., and Henning, Allen B.: Lateral Stability Characteristics at Low Lift Between Mach Numbers of 0.85 and 1.15 of a Rocket-Propelled Model of a Supersonic Airplane Configuration Having a Tapered Wing With Circular-Arc Sections and 40° Sweepback. NACA RM L55A31, 1955.

4. Malvestuto, Frank S., Jr., Margolis, Kenneth, and Ribner, Herbert S.: Theoretical Lift and Damping in Roll at Supersonic Speeds of Thin Sweptback Tapered Wings With Streamwise Tips, Subsonic Leading Edges, and Supersonic Trailing Edges. NACA Rep. 970, 1950. (Supersedes NACA TN 1860.)

5. Martin, John C., and Jeffreys, Isabella: Span Load Distributions Resulting From Angle of Attack, Rolling, and Pitching for Tapered Sweptback Wings With Streamwise Tips - Supersonic Leading and Trailing Edges. NACA TN 2643, 1952.

6. Anon.: Flying Qualities of Piloted Airplanes. Military Specifications, MIL-F-8785 (ASG) Sept. 1, 1954.

[redacted]

TABLE I.- PHYSICAL CHARACTERISTICS OF A 0.125-SCALE MODEL OF THE McDONNELL F-101A AIRPLANE

Wing:	
Area (theoretical), sq ft	5.75
Span, ft	4.97
Aspect ratio	4.28
Mean aerodynamic chord, ft	1.28
Taper ratio	0.28
Sweepback of leading edge, deg	41.12
Sweepback of trailing edge, deg	19.42
Incidence angle (with respect to model center line), deg	1.0
Dihedral angle, deg	0
Root thickness (theoretical), percent chord	6.67
Tip thickness, percent chord	5.71
Horizontal tail:	
Area, sq ft	1.17
Span, ft	1.97
Aspect ratio	3.30
Mean aerodynamic chord, ft	0.62
Taper ratio	0.46
Sweepback of leading edge, deg	39.80
Sweepback of trailing edge, deg	20.93
Dihedral angle, deg	10.00
Hinge-line location, percent of tail mean aerodynamic chord	26.5
Root airfoil section	NACA 65A007 modified
Tip airfoil section	NACA 65A006 modified
Tail length (25 percent wing MAC to 25 percent tail MAC), ft	3.69
Fuselage:	
Length, ft	8.38
Width (maximum), ft	0.96
Height (maximum), ft	0.88
Maximum cross-sectional area, sq ft	0.66
Ducts (one side):	
Inlet capture area, sq ft	0.0625
Exit area, sq ft	0.0474
Area at compressor face (excluding area blocked by accessory housing), sq ft	0.0802
Vertical tail:	
Area above fuselage (dorsal fin excluded), sq ft	1.18
Span, ft	0.94
Mean aerodynamic chord (theoretical), ft	1.46
Aspect ratio (theoretical)	0.66
Sweepback angle at leading edge, deg	52.00
Sweepback angle at trailing edge, deg	16.60
Airfoil section	NACA 65A007
Weight and balance:	
Weight, lb	379.4
Wing loading, lb/sq ft	66.0
Center-of-gravity location, percent MAC	17.3
Moment of inertia in roll, slug-ft^2	3.57
Moment of inertia in pitch, slug-ft^2	46.30
Moment of inertia in yaw, slug-ft^2	47.78
Inclination of principal axis, deg below the nose	4.2

[redacted]

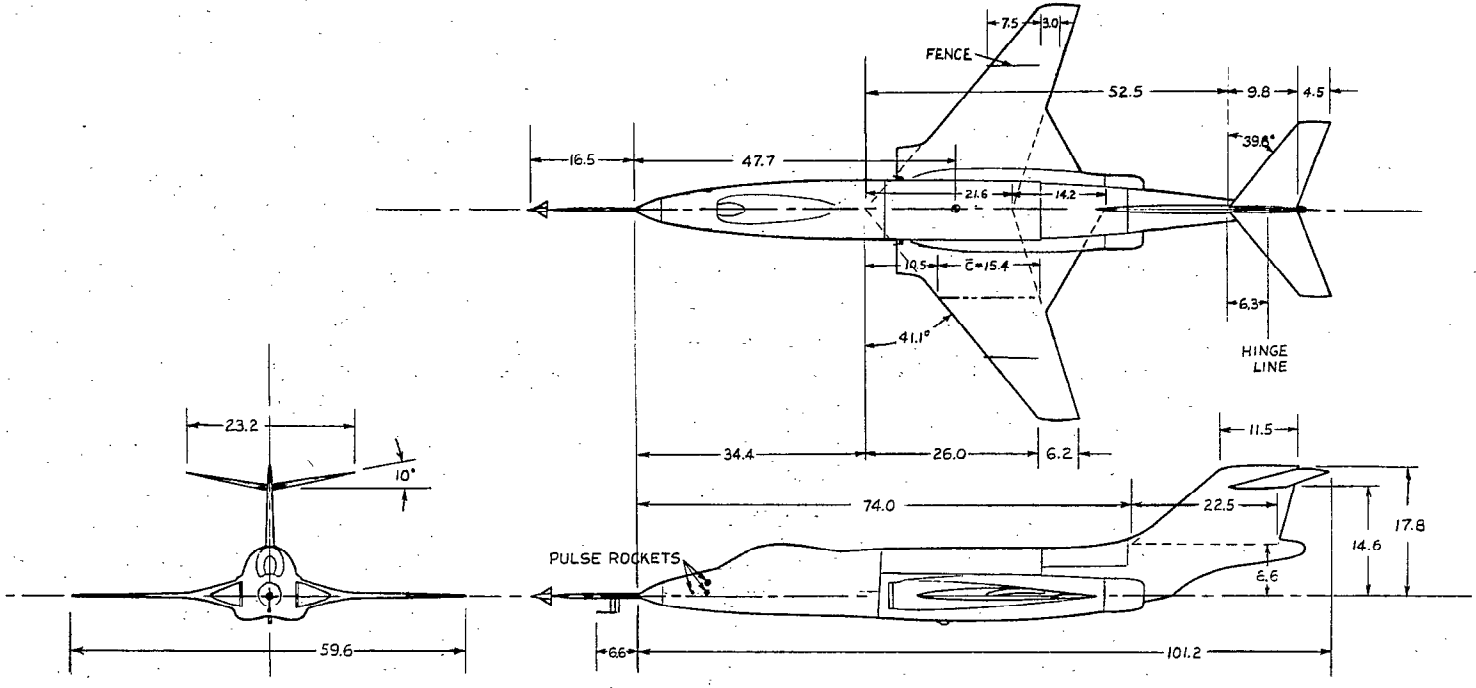

Figure 1.- Three-view drawing of model. Broken lines indicate plan form of theoretical wing. All dimensions are in inches.

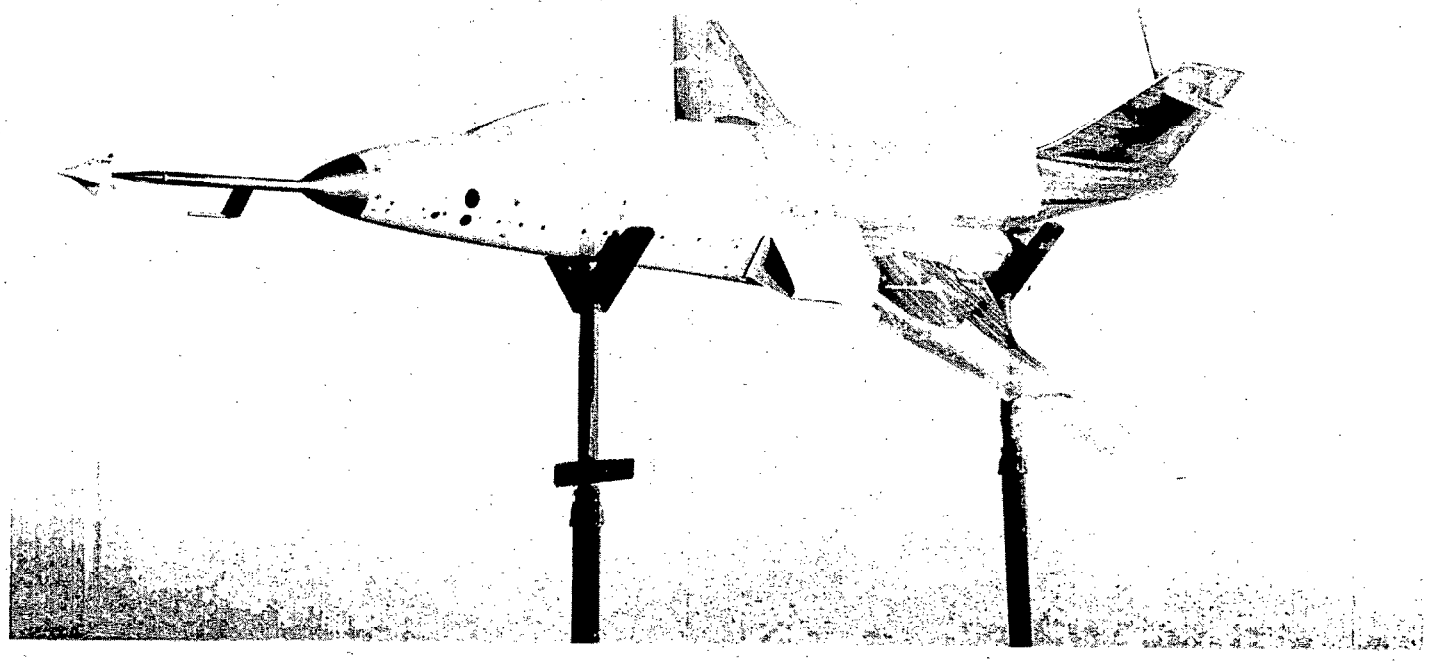

L-87605.1

(a) Free-flight rocket model.

Figure 2.- Photographs of the rocket model.

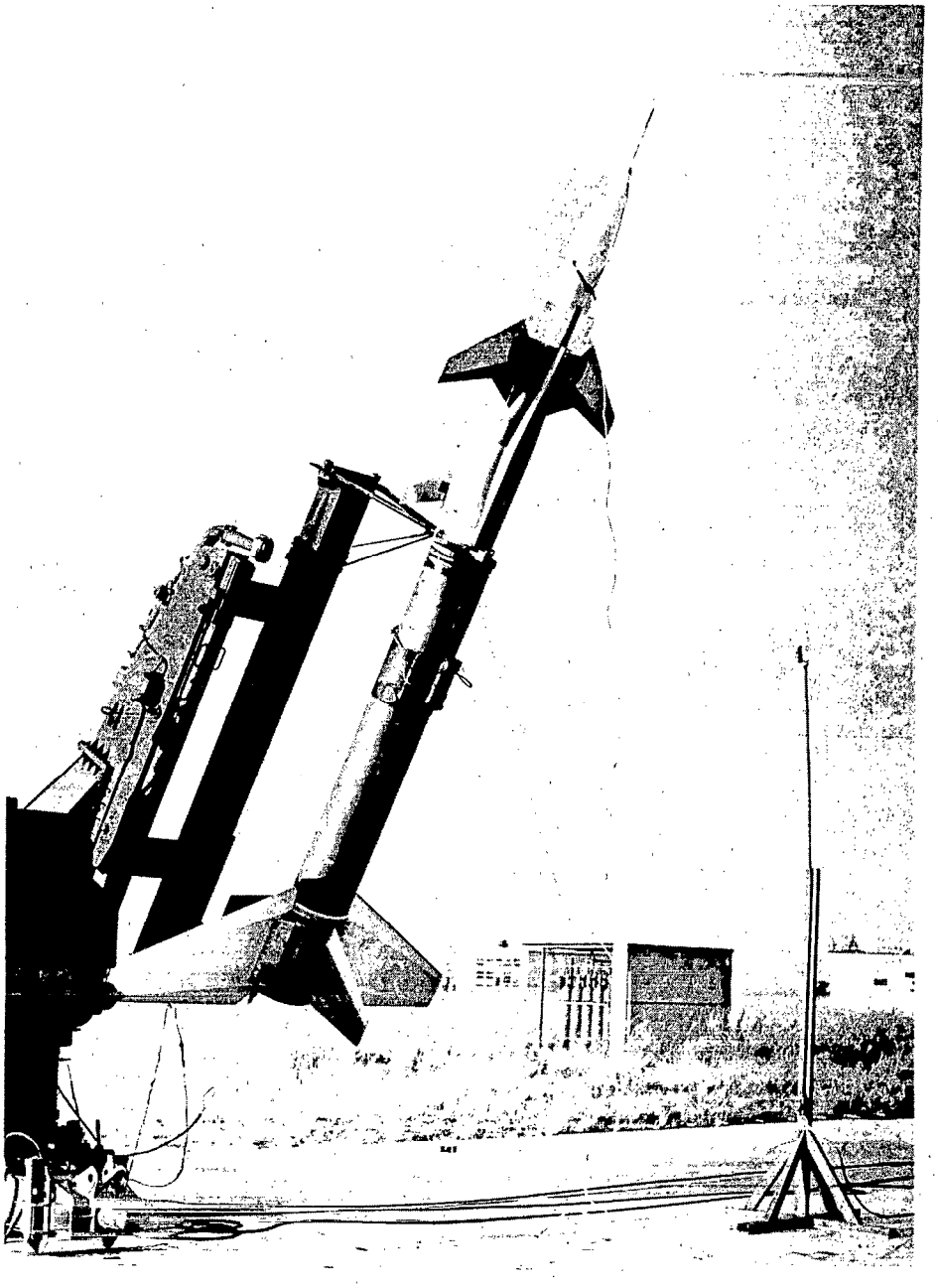

L-87730.1

(b) Model and booster on launcher.

Figure 2.- Concluded.

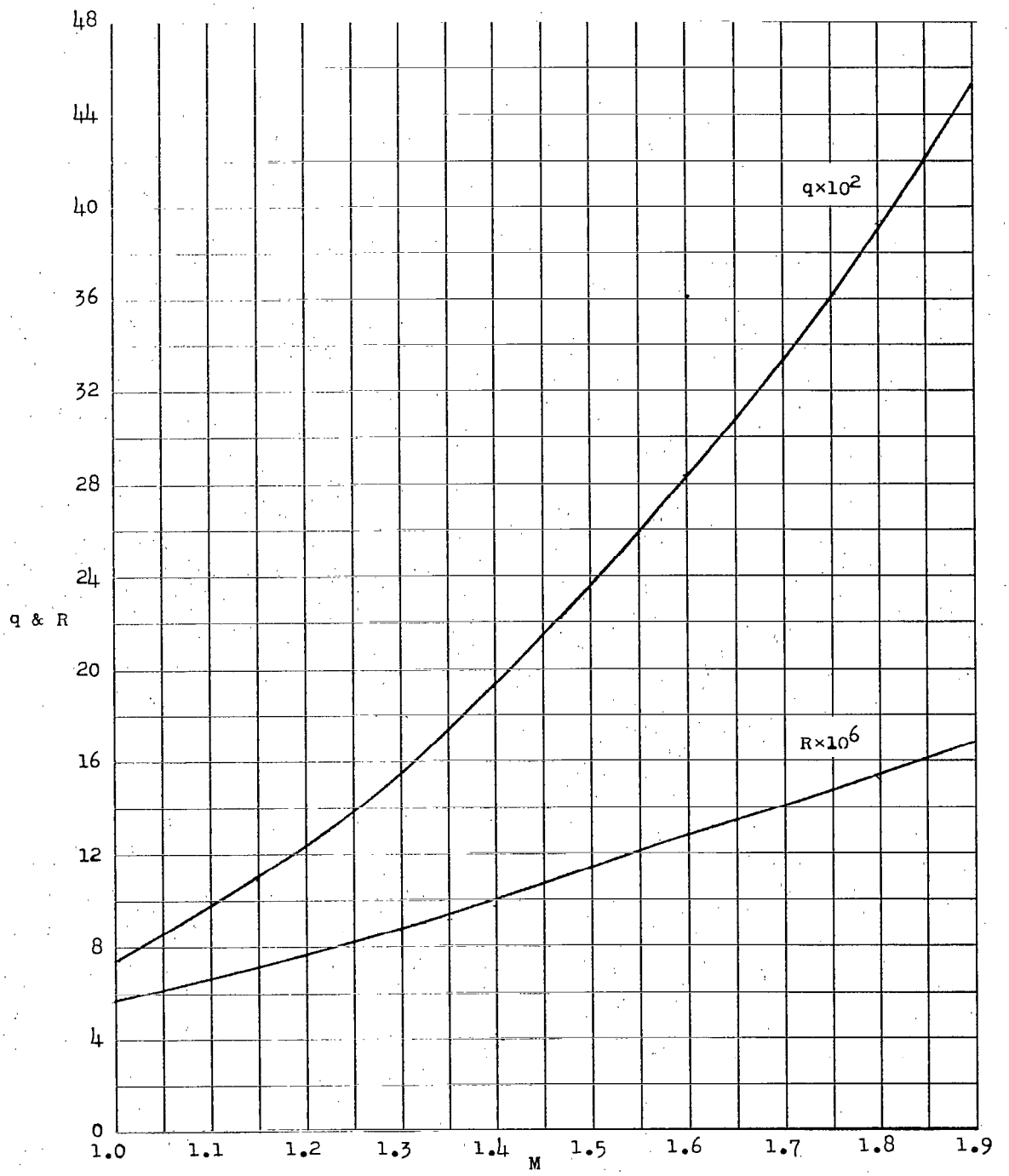

Figure 3.- Variation of test dynamic pressure and Reynolds number with Mach number.

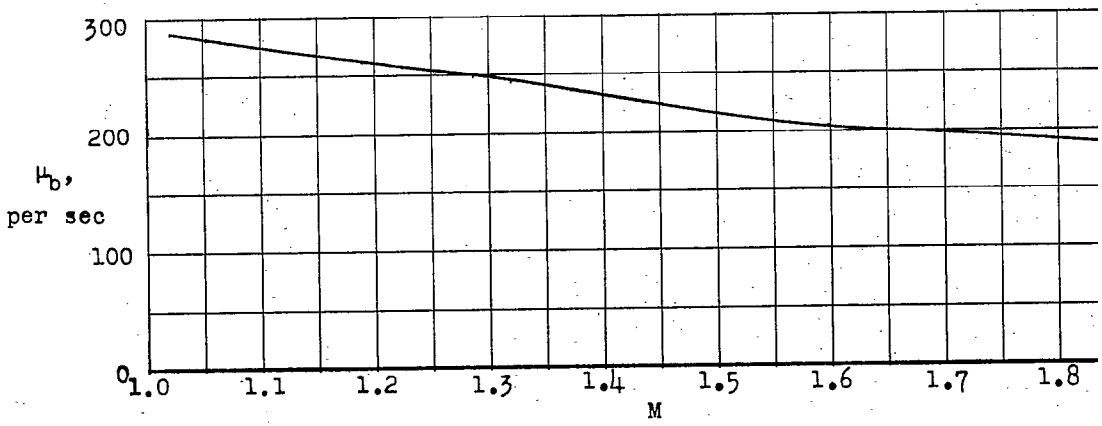

(a) Mass parameter of the model.

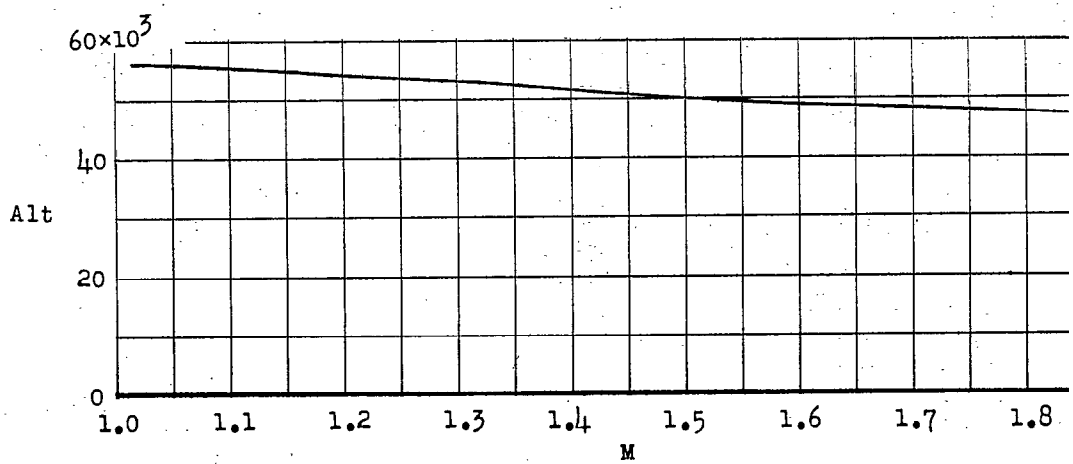

(b) Altitude of full-scale airplane having same mass paramete

Figure 4.- Model mass-density parameter and equivalent full-scale altitude.

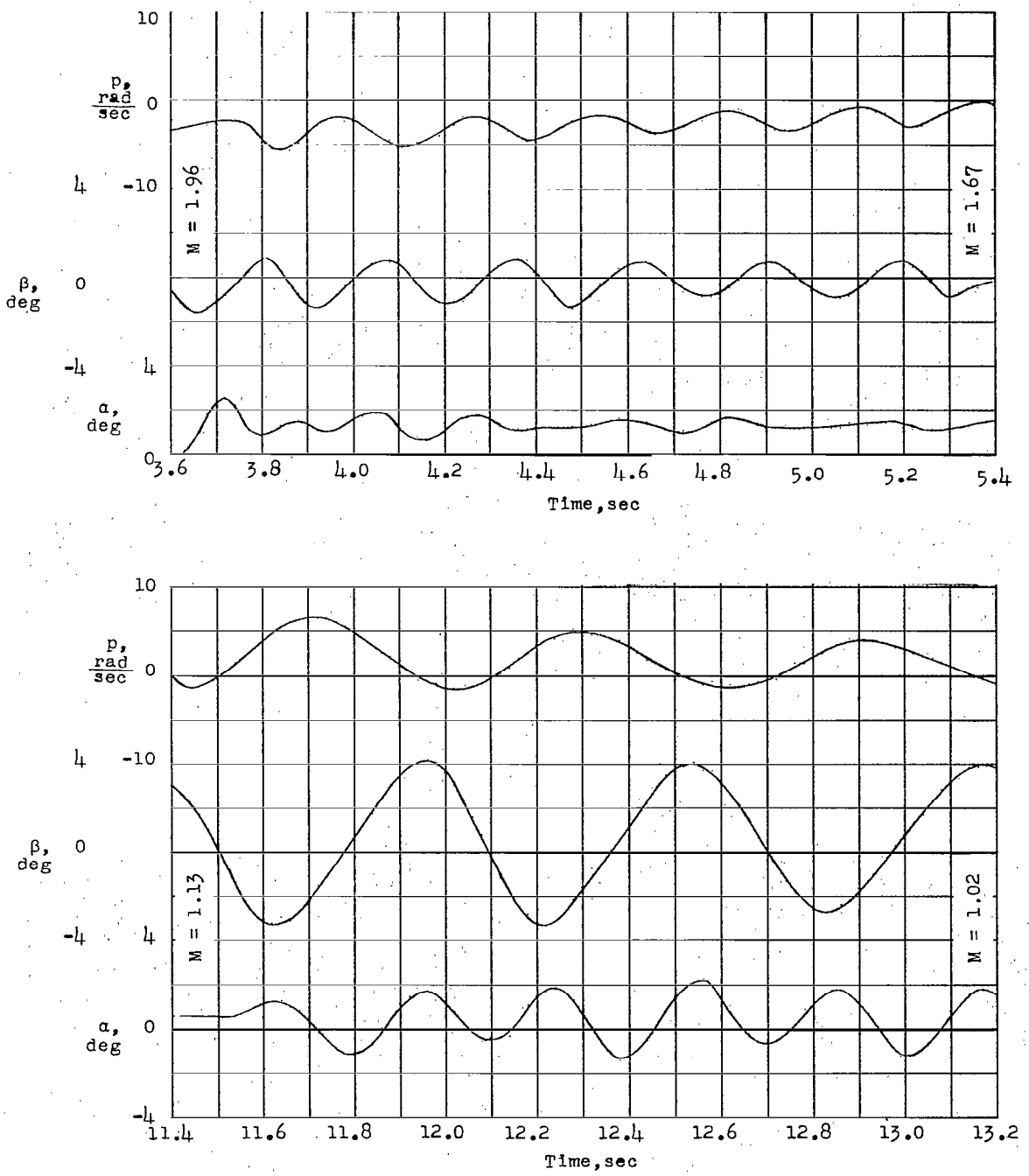

Figure 5.- Time history of some of the quantities measured.

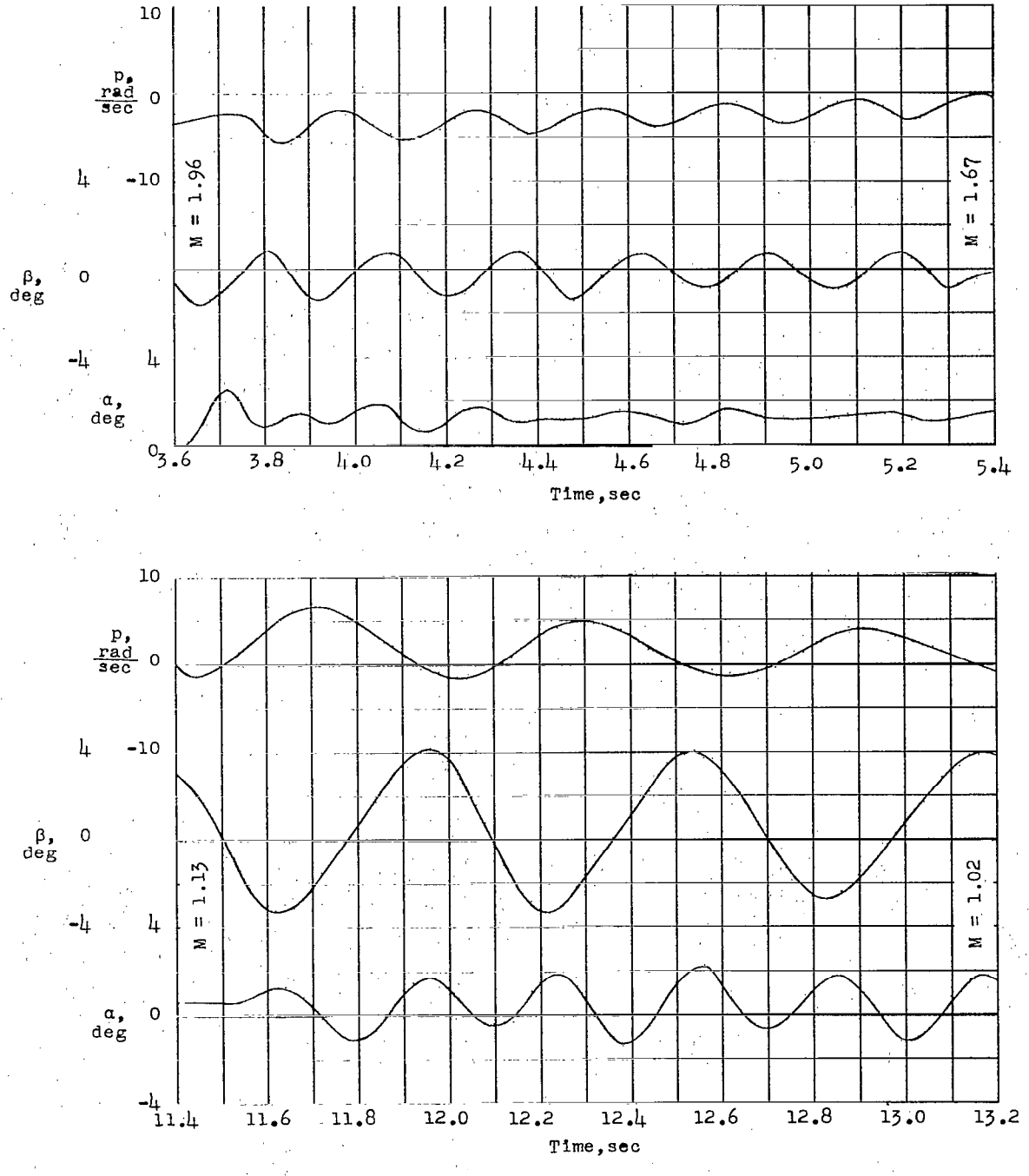

Figure 5.- Time history of some of the quantities measured.

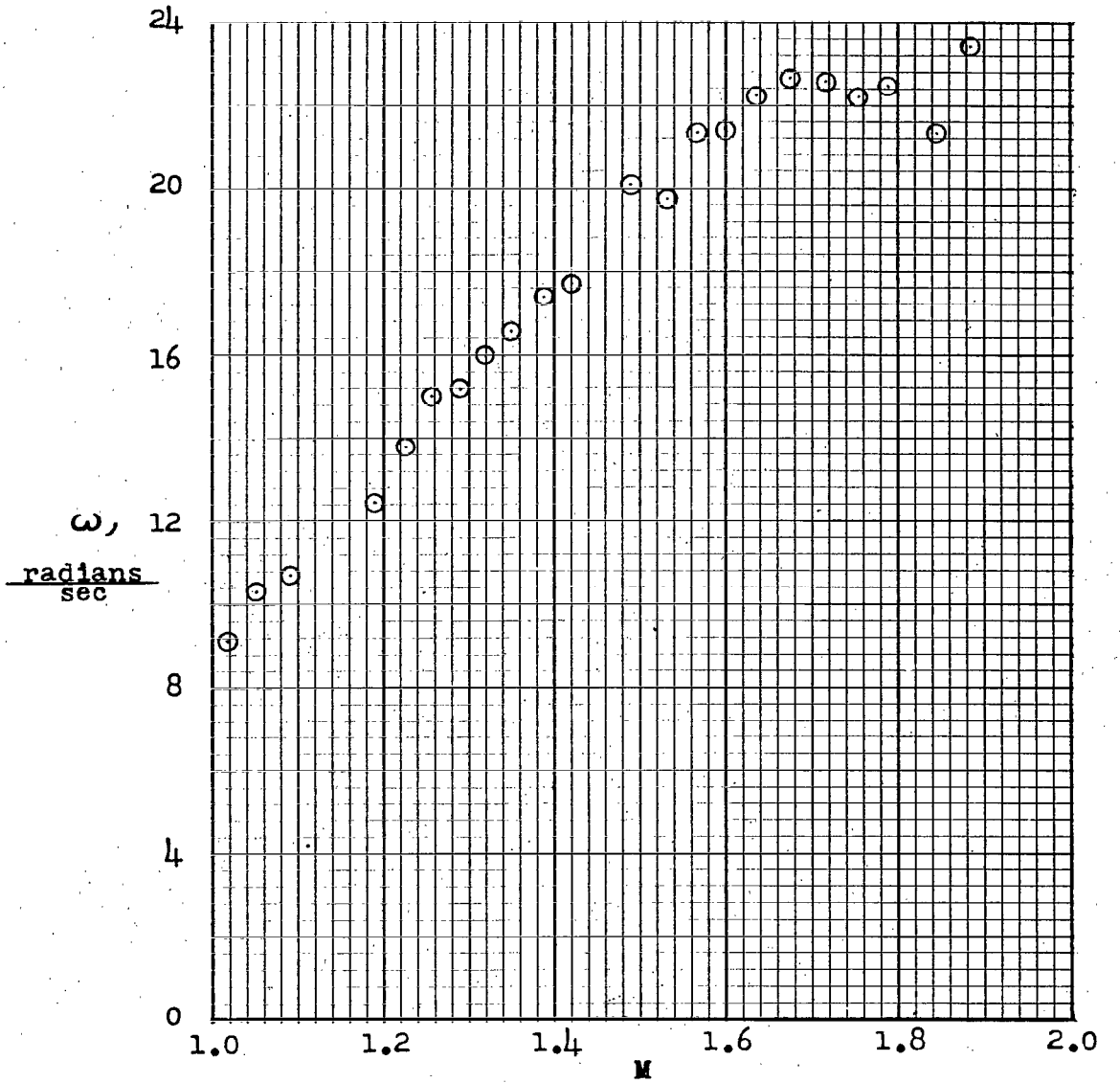

Figure 6.- Frequency of Dutch roll oscillations.

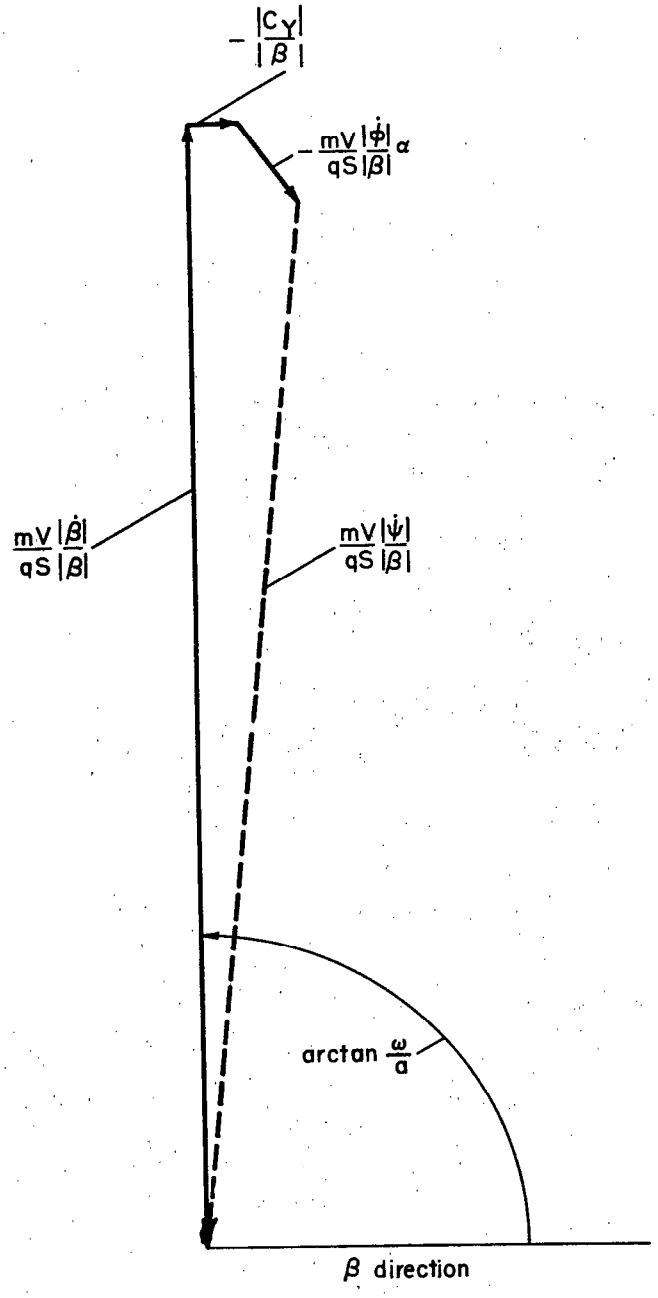

Sideforce equation:

$$\frac{mV|\dot{\beta}|}{qS|\beta|}+\frac{mV|\dot{\psi}|}{qS|\beta|}-\frac{mV|\dot{\phi}|}{qS|\beta|}\alpha-\frac{|C_Y|}{|\beta|}=0$$

Figure 7.- Typical vector solution; body axis system.

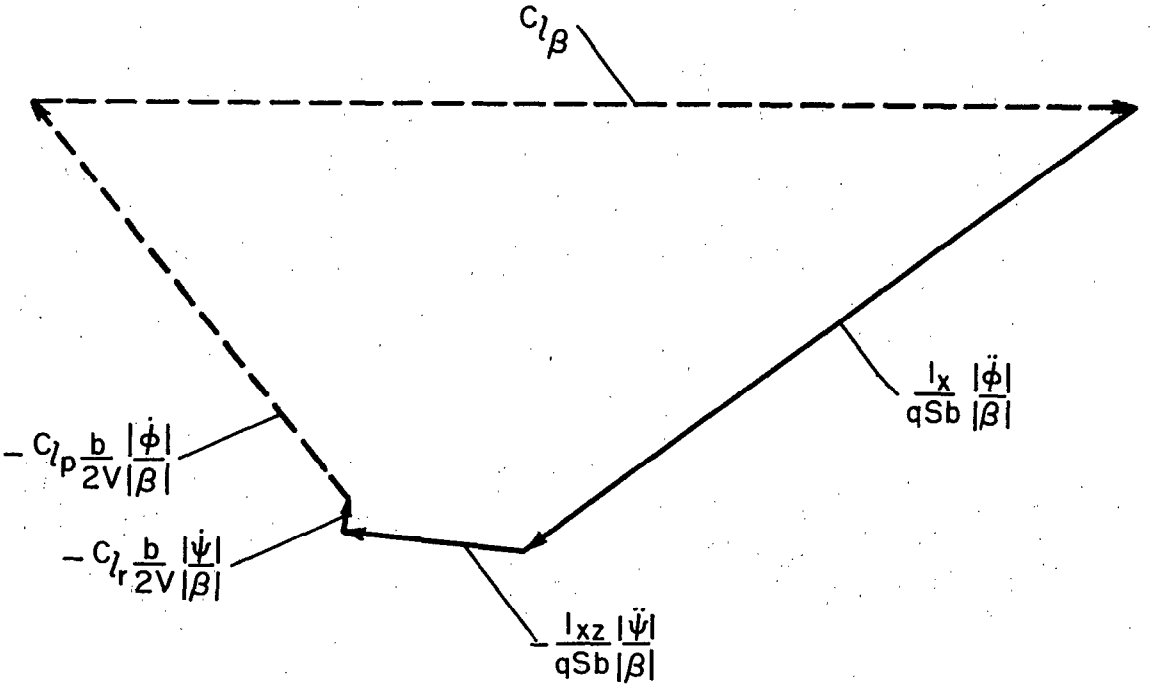

Rolling-moment equation:

$$\frac{I_x}{qSb}\left|\frac{\ddot{\phi}}{\beta}\right| - \frac{I_{xz}}{qSb}\left|\frac{\ddot{\psi}}{\beta}\right| - C_{l_r}\frac{b}{2V}\left|\frac{\dot{\psi}}{\beta}\right| - C_{l_p}\frac{b}{2V}\left|\frac{\dot{\phi}}{\beta}\right| - C_{l_\beta} = 0$$

Figure 7.- Continued.

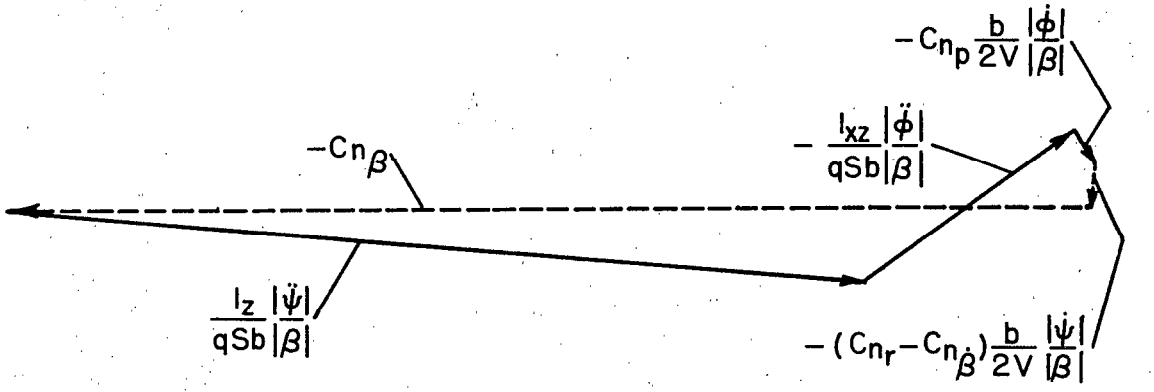

Yawing-moment equation

$$\frac{I_z}{qSb} \frac{|\ddot{\psi}|}{|\beta|} - \frac{I_{xz}}{qSb} \frac{|\ddot{\phi}|}{|\beta|} - Cn_p \frac{b}{2V} \frac{|\dot{\phi}|}{|\beta|} - (Cn_r - Cn_{\dot{\beta}}) \frac{b}{2V} \frac{|\dot{\psi}|}{|\beta|} - Cn_\beta = 0$$

Figure 7.- Concluded.

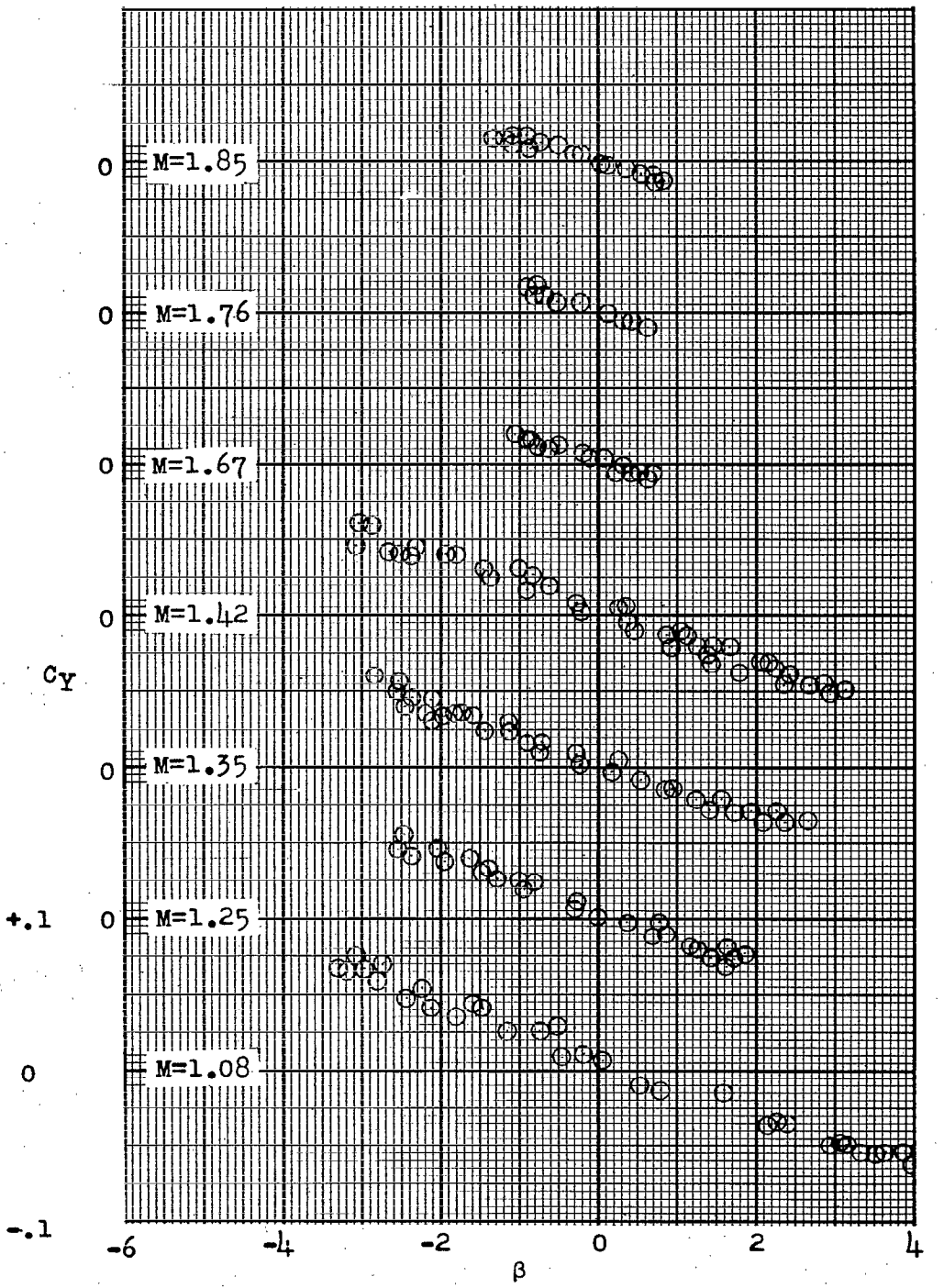

Figure 8.- Variation of side-force coefficient with angle of sideslip.

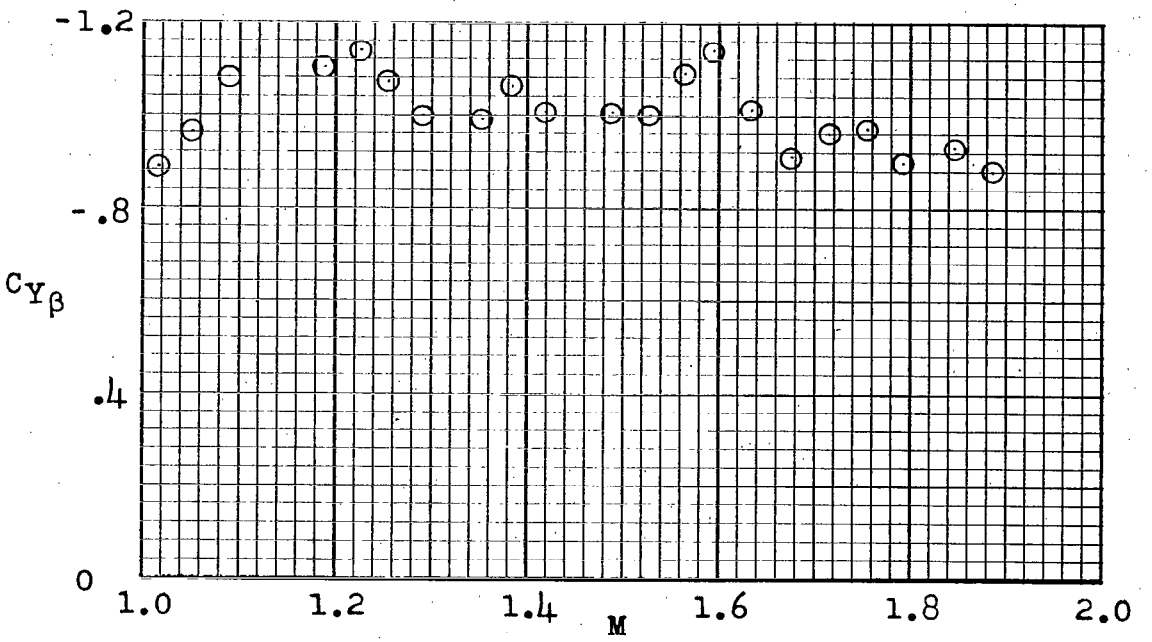

Figure 9.- Side force due to angle-of-sideslip derivative.

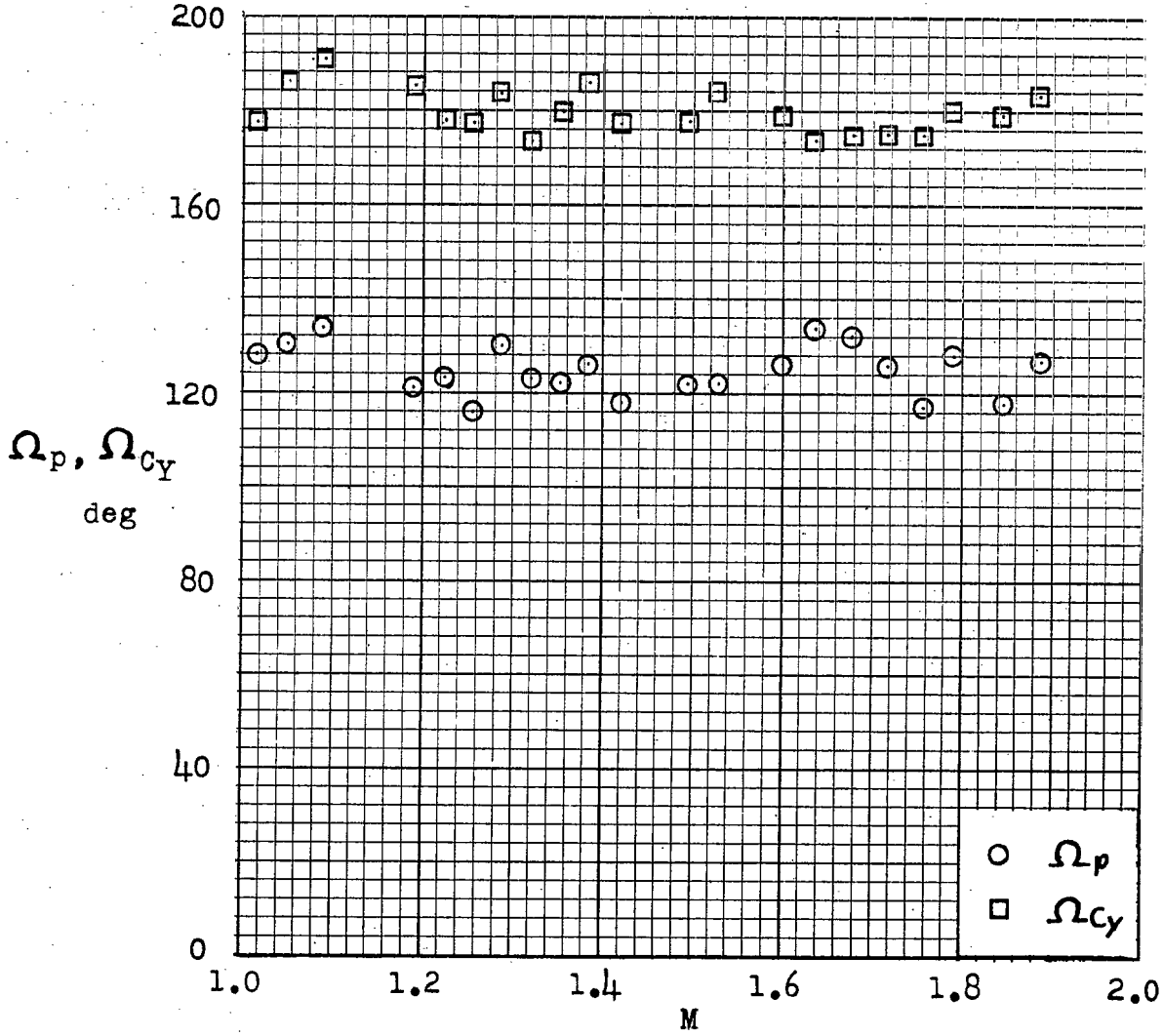

Figure 10.- Phase angles of roll rate and side-force coefficient to angle of sideslip.

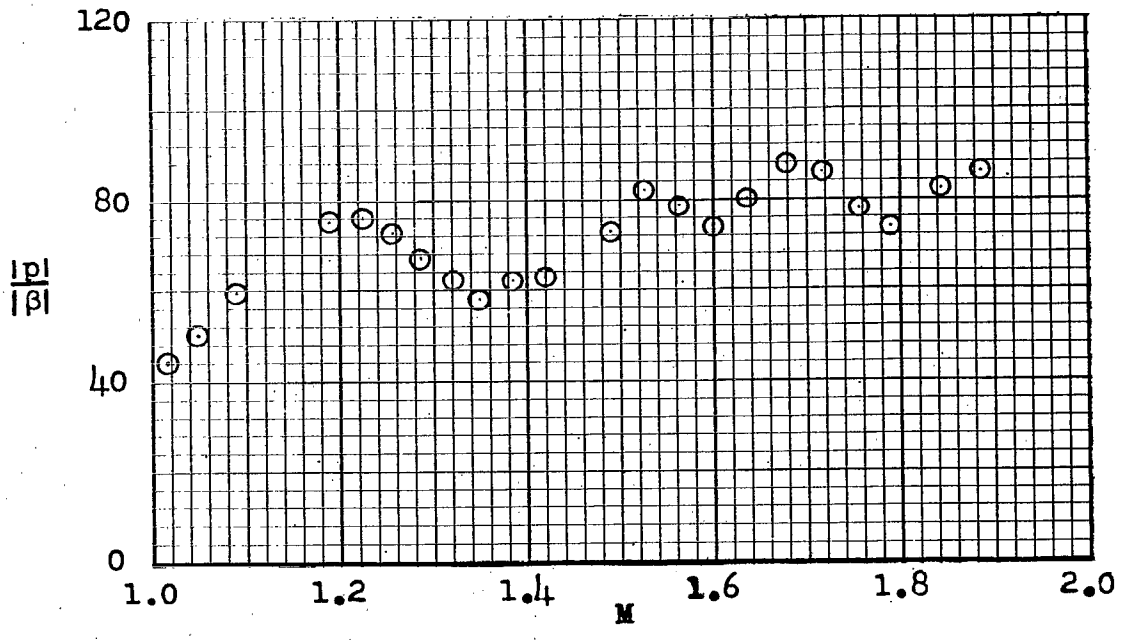

Figure 11.- Amplitude ratio of roll rate to angle of sideslip.

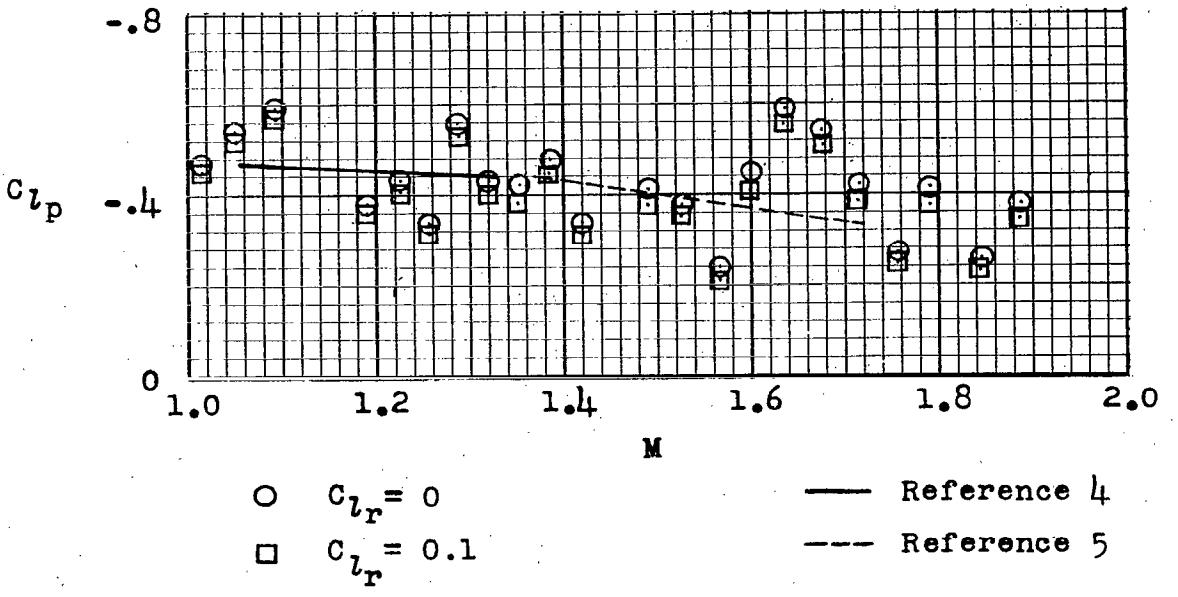

Figure 12.- Roll-damping derivative.

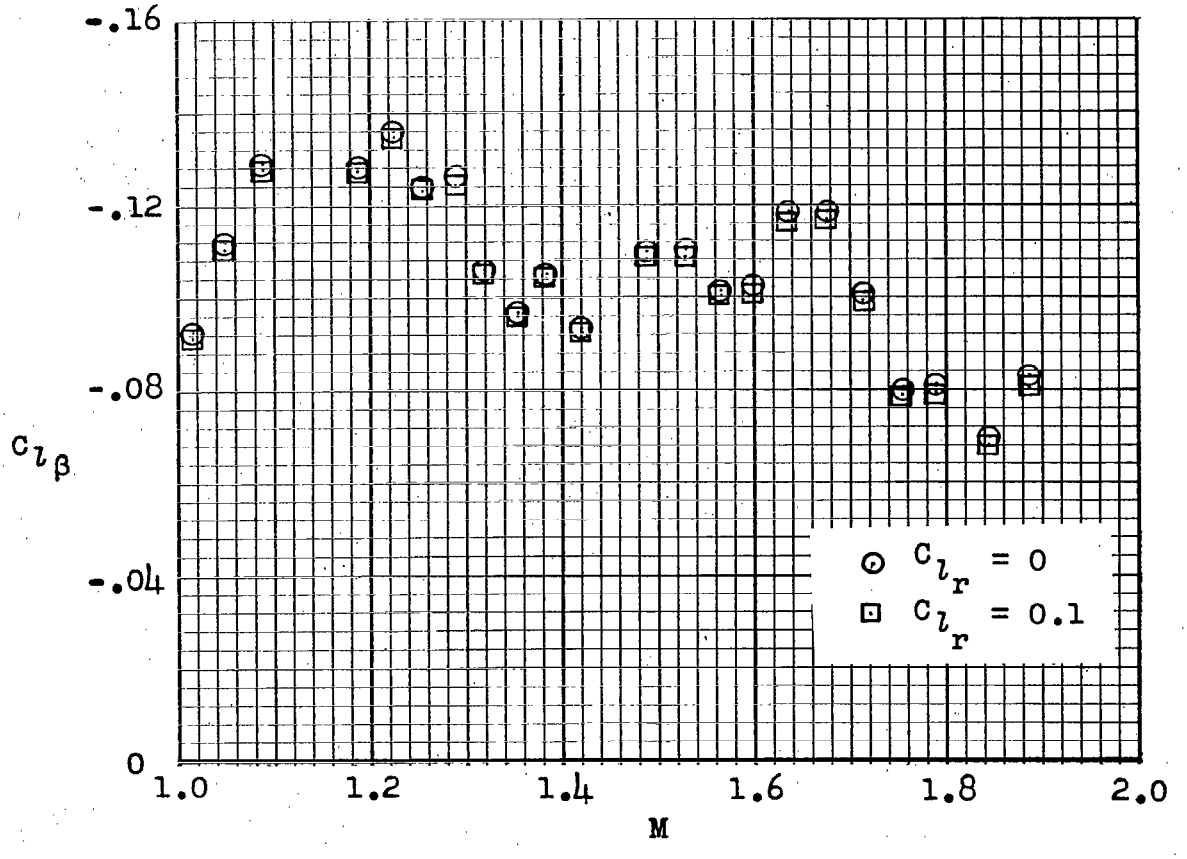

Figure 13.- Dihedral-effect derivative.

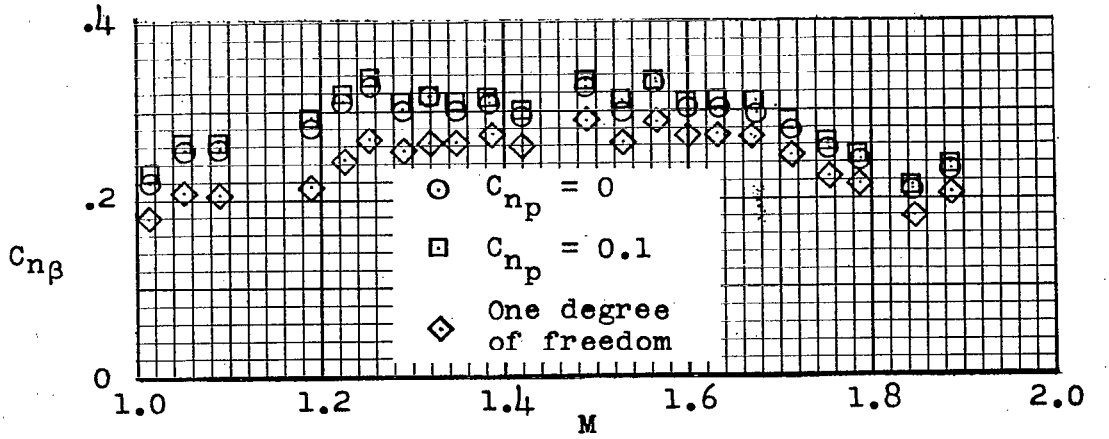

Figure 14.- Static lateral stability.

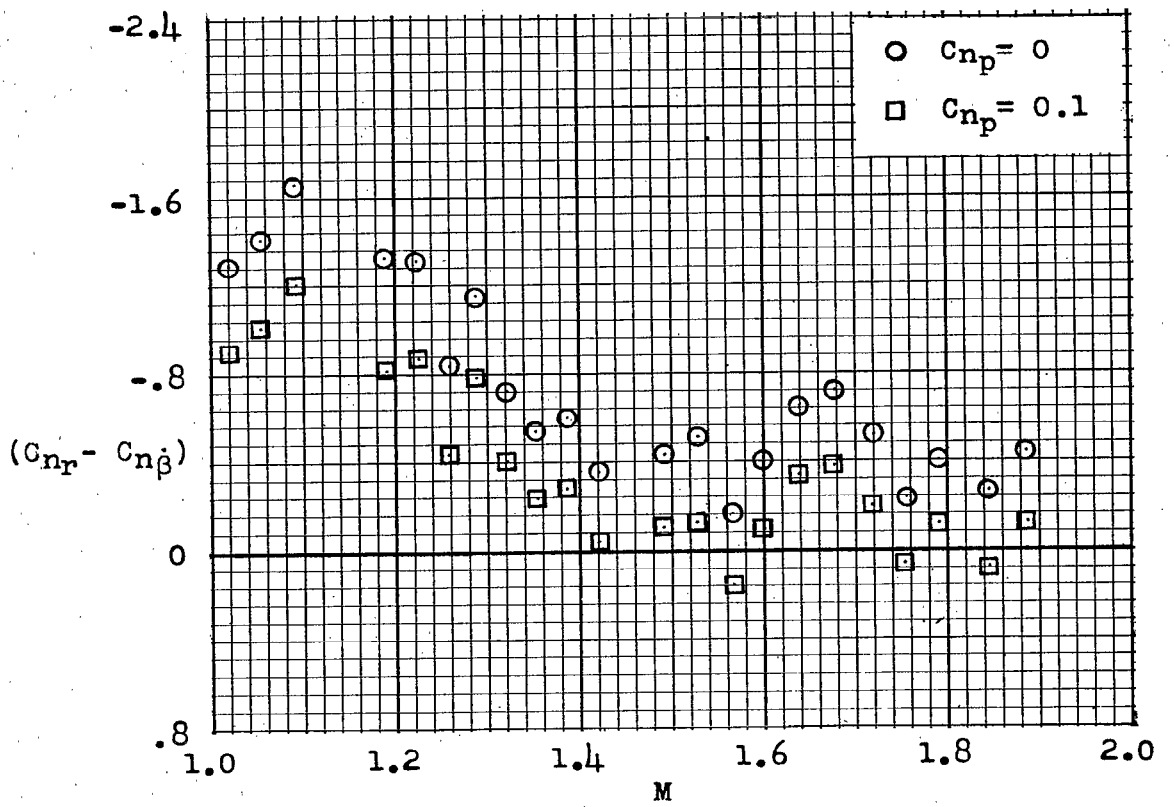

Figure 15.- Dynamic-lateral-stability derivative.

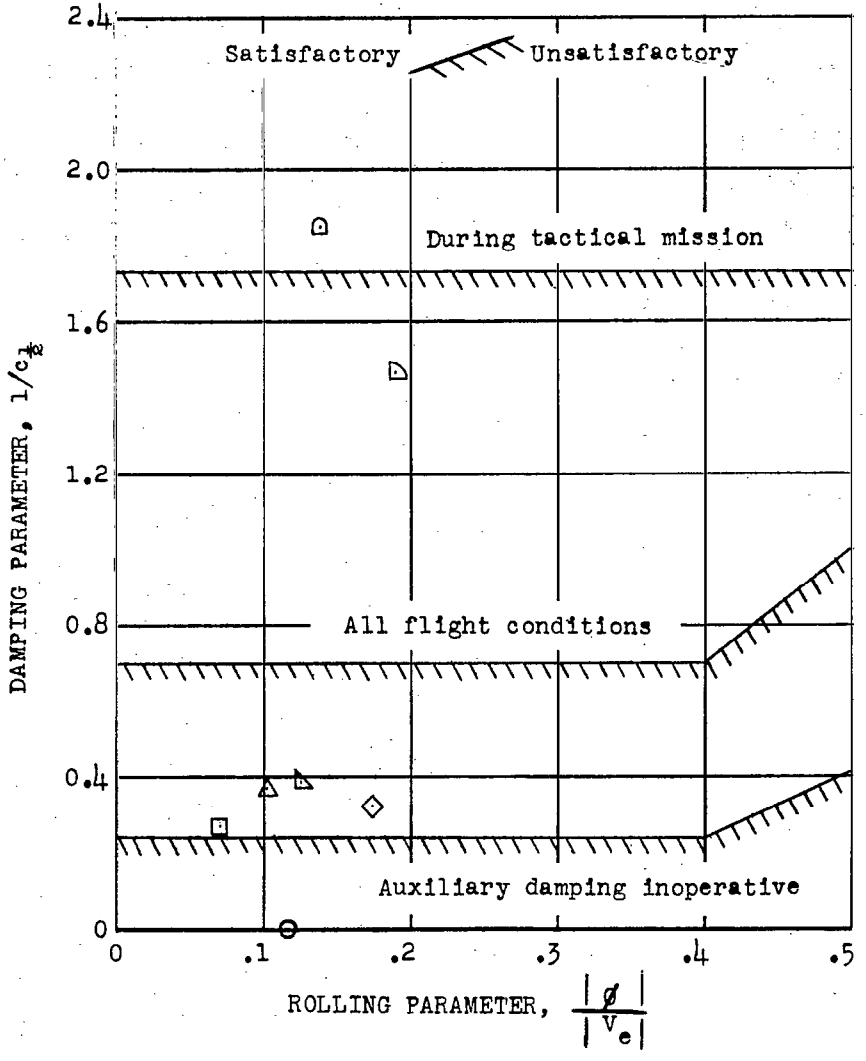

Model

○ M = 1.845 Measured

□ M = 1.845 Calculated with k_x/b, k_z/b, and k_{xz}/b, same as airplane.

Calculated Airplane[a]

◇ M = 1.845 Altitude 47,000 ft so that $\left(\frac{m}{\rho Sb}\right)_{airplane} = \left(\frac{m}{\rho Sb}\right)_{model}$.

△ M = 1.845 Altitude 25,000 ft

◺ M = 1.420 Altitude 25,000 ft

◺ M = 1.225 Altitude 25,000 ft

◺ M = 1.017 Altitude 25,000 ft

(a) Derivatives used were those obtained from model assuming $C_{n_p} = C_{l_r} = 0$.

Level flight angle of attack. Mass characteristics Table I.

Figure 16.- Calculated damping of the lateral-directional oscillations of the airplane at several assumed flight conditions.

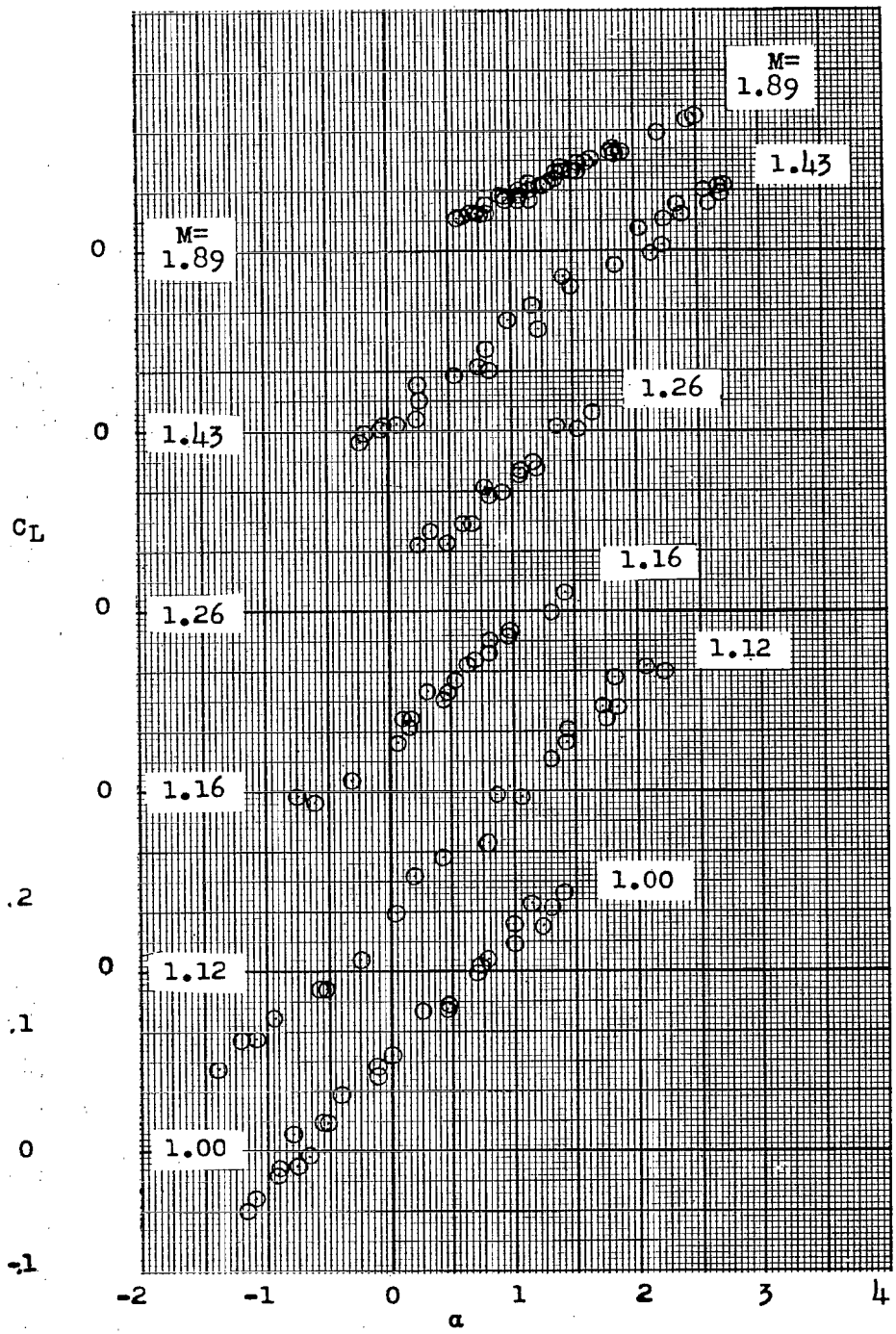

Figure 17.- Variation of lift coefficient with angle of attack.

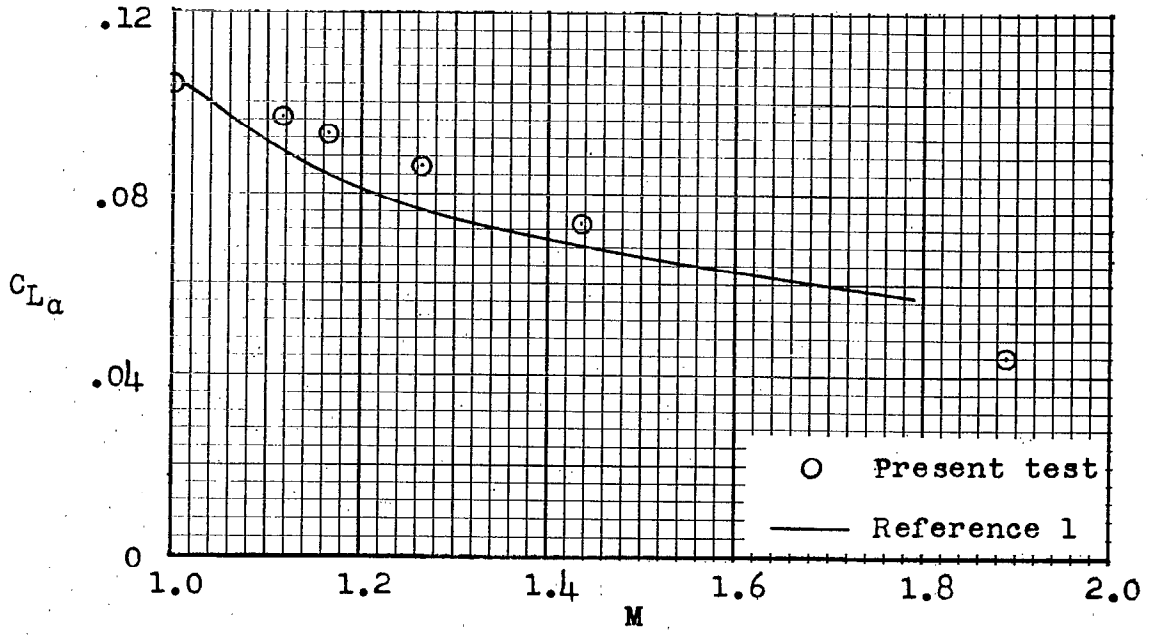

Figure 18.- Lift-curve slope.

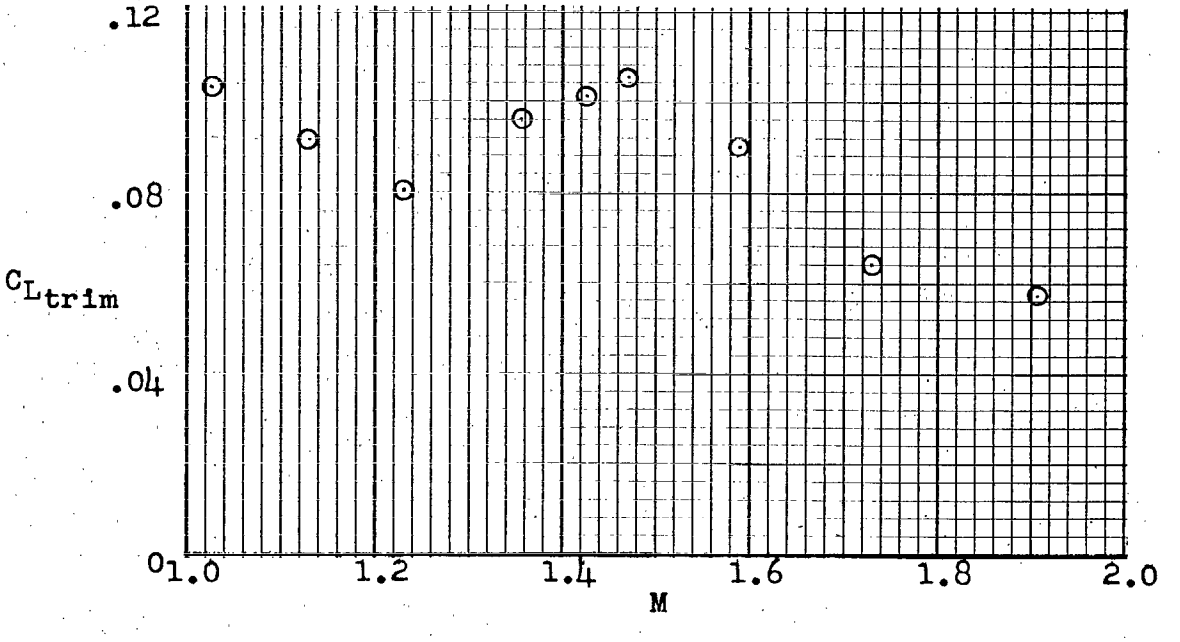

Figure 19.- Trim lift coefficient.

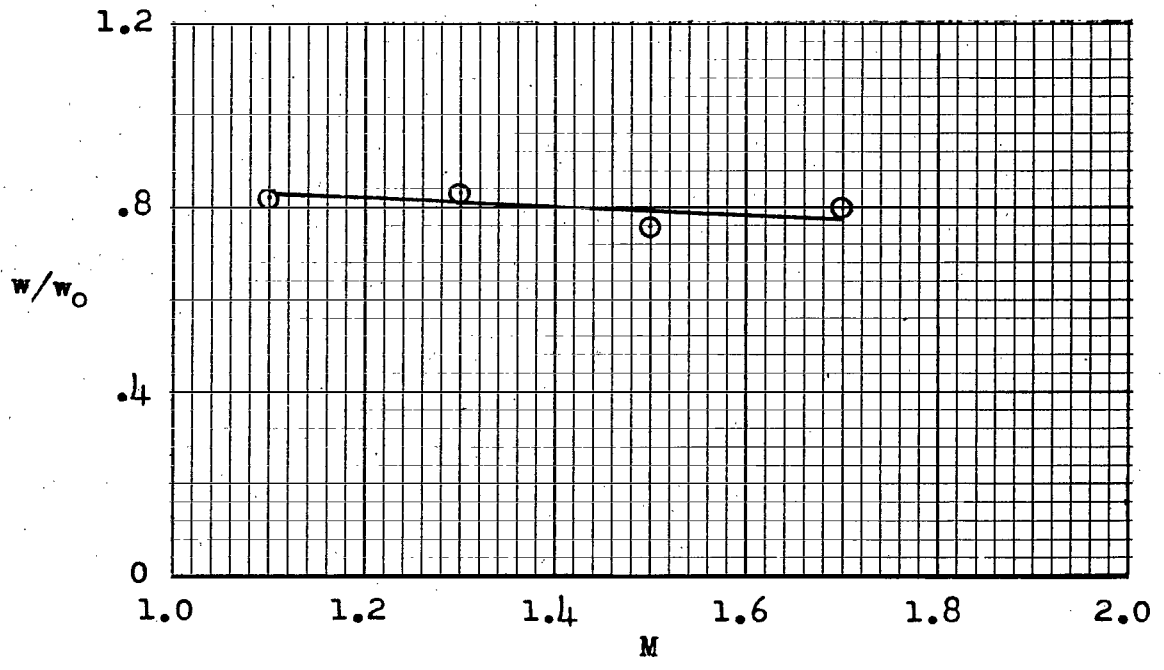

Figure 20.- Duct mass-flow ratio.

[redacted]

INDEX

ABSTRACT

A model of F-101A was flight tested at the Wallops Island Research Station by using pulse rockets to produce lateral disturbances. Vector analyses were made to find lateral stability derivatives. A comparison of model damping with the calculated damping of the airplane was made.

[redacted]